High-Bandwidth Shielded Rogowski Coil Current Sensor for SiC MOSFET Power Module

Wen Zhang
Min H. Kao Dept. of EECS
The University of Tennessee
Knoxville, USA
wen.zhang@utk.edu

Fred Wang
Min H. Kao Dept. of EECS
The University of Tennessee
Oak Ridge National Lab.
Knoxville, USA
fred.wang@utk.edu

Bernhard Holzinger
Keysight Technologies
Böblingen, Germany
bernhard_holzinger@keysight.com

2021 IEEE Applied Power Electronics Conference and Exposition (APEC) | 978-1-7281-8949-9/21/$31.00 ©2021 IEEE | DOI: 10.1109/APEC42165.2021.9487370

***Abstract*—Existing current sensors suffer from insufficient measurement bandwidth or large insertion area to continuously monitor the switching transient current of wide-bandgap devices. A combinational Rogowski coil concept is proposed here, where the self-integrating region of a shielded Rogowski coil is combined with its differentiating region. The overall measurement bandwidth is effectively extended by the self-integrating region. The design methodology for the shielded Rogowski coil, especially the parasitic elements and error analysis, is discussed. Finally, a prototype is demonstrated with a sensitivity is 5.0 mΩ and a bandwidth of 200 MHz. The measurement in a SiC power module double pulse shows it can faithfully capture the transient current while introducing little interference.**

***Index Terms*—Current sensor, Rogowski coil, SiC MOSFET, double pulse test**

I. Introduction

Wide-bandgap devices exhibit much faster switching speed than Silicon counterparts. Recent packaging improvements have enabled smaller and smaller power loop inductance for SiC MOSFET power modules [1], [2]. The switching transient oscillation frequency determined by the parasitic capacitance and inductance is therefore also increased. In order to capture the current waveform faithfully, the current sensor or probe must possess sufficiently high measurement bandwidth. Furthermore, because the switching transient performance of SiC MOSFETs is highly dependent on the power loop parasitic inductance [3], the insertion inductance due to the extra power loop area to accommodate the current sensor must be small.

Resistive current shunts can achieve very high bandwidth up to several GHz but are limited to pulse operation and not capable of continuous measurement due to heat dissipation [4], [5]. Current transformers can also achieve up to 250 MHz measurement bandwidth but the cross-sectional area is quite large due to the magnetic core saturation limitation [6]. Rogowski coils are another widely used type of current sensor based on the Faraday's induction low [7]. The helix coil directly measures the derivative of the current, which is then reconstructed by a passive or active integrating circuit [8]. The state-of-the-art commercial Rogowski coil has a small cross-sectional area but the measurement bandwidth is only 50 MHz. A two-turn Rogowski coil with up to 225 MHz bandwidth is demonstrated in [9], but numerical integration with oscilloscope is required. [10] proposed an integrated Rogowski coil for a GaN power stage but the exact measurement bandwidth is not provided.

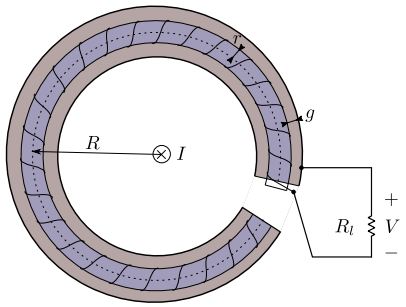

Fig. 1. Simplified schematic of a shielded Rogowski coil.

On the other hand, shielded Rogowski coils can exhibit self-integrating characteristic and a linear gain within a relatively high frequency region [11]. A simplified schematic of the shielded Rogowski coil is shown in Fig. 1. Instead of a single return turn going through the center of the coil, a layer of copper shielding covers the entire coil from outside. The parasitic capacitance between the helix coil winding and the shielding can achieve integration in the high frequency range [8], [12]. In the aforementioned literature, the cross-sectional areas are relatively large and therefore unsuitable for SiC MOSFET measurement.

In this paper, the combinational Rogowski coil concept is proposed, which utilizes both the self-integrating and differentiating regions of a shielded Rogowski coil. The measurement bandwidth is greatly increased, while the cross-sectional area is kept small to minimize the extra insertion inductance. The design and fabrication methodology is discussed, including the parasitic element model and error analysis due to eccentricity and tilting. Network analyzer measurements verify the measurement bandwidth of hand-made prototypes is extended to 200 MHz. Double pulse tests with a SiC MOSFET power module further shows the coil can faithfully capture the waveform while introducing little extra parasitic inductance.

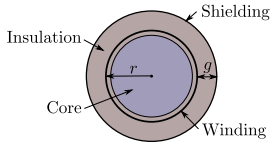

Fig. 2. Shielded Rogowski coil cross-sectional view.

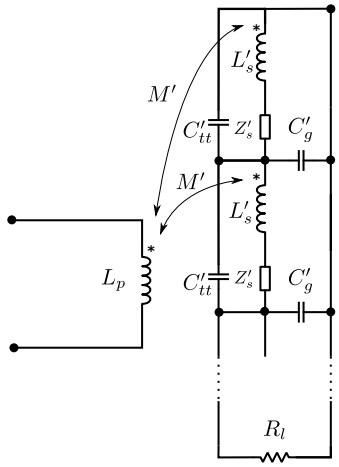

Fig. 3. Distributed element circuit model of a shielded Rogowski coil.

II. Shielded Rogowski Coil Self-Integrating Characteristics and Parasitics Model

A. Self-integrating characteristics

A more detailed view of the shielded Rogowski coil cross section is shown in Fig. 2. The helix coil winding is wound around a donut shaped amagnetic core. The winding major and minor radii are denoted as R and r, respectively. The winding is wrapped around an insulator with a thickness of g. Finally, the copper shielding is attached all around the insulator. The copper shielding is connected to one end of the winding. The other terminal and shielding are terminated with a loading resistance of R_l.

Assuming the primary side conductor is placed at the center of the coil, the equivalent distributed element circuit model for the shielded Rogowski coil is then shown in Fig. 3. The coil self-inductance is denoted as L_s, the winding-to-shielding parasitic capacitance C_g, the turn-to-turn capacitance C_{tt}, the AC impedance of the winding Z_s, and the mutual inductance between primary and Rogowski coil M. The superscript prime represents the per-unit-length value in Fig. 3. Assuming the AC resistance Z'_s and turn-to-turn capacitance C'_{tt} can be neglected, the transfer impedance Z_t is then given by [11],

$$Z_t = \frac{V}{I} = \frac{M}{L_s} \cdot \frac{1}{R_l^{-1} - jZ_0^{-1}\cot\left(\omega\sqrt{L_sC_g}\right)}, \tag{1}$$

where $Z_0 = \sqrt{\frac{L_s}{C_g}}$ is the wave impedance of the coil.

A transfer impedance example over the frequency spectrum is shown in Fig. 4. The transfer impedance clearly shows distinctive behavior in different frequency regions. In the lower frequency, the coil appears differentiating. Inspecting (1), in

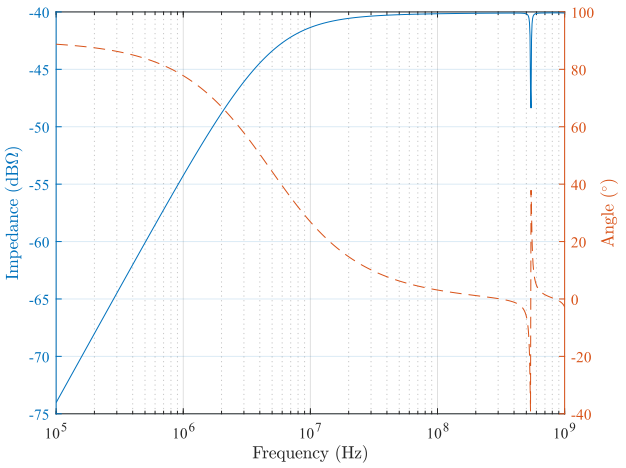

Fig. 4. Transfer impedance of a shielded Rogowski coil.

the lower frequency spectrum, when $Z_0^{-1}\cot\left(\omega\sqrt{L_sC_g}\right) \gg R_l^{-1}$, the coil output appears differentiating like a normal Rogowski coil,

$$Z_t \approx j\omega M. \tag{2}$$

As the frequency get higher, Fig. 4 shows that the coil output becomes linear. When $Z_0^{-1}\cot\left(\omega\sqrt{L_sC_g}\right) \ll R_l^{-1}$, the output of the coil will be proportional to the primary side current and appears linear or self-integrating,

$$Z_t \approx \frac{R_l M}{L_s}. \tag{3}$$

Because of the periodic nature of the cot function, the linear response region appears in many frequency bands in the higher frequency spectrum. The first frequency band immediately after the differentiating region can be used for current sensing purpose. The primary side current signal starts being distorted at the first oscillation point, and the rest of the high frequency spectrum cannot be used to reconstruct the current signal. The start and end frequency of the first self-integrating band can be found by equating the previous frequency band conditions,

$$BW_L = \frac{\arctan\frac{R_l}{\sqrt{L_s/C_g}}}{2\pi\sqrt{L_sC_g}}, \tag{4}$$

$$BW_H = \frac{\pi - \arctan\frac{R_l}{\sqrt{L_s/C_g}}}{2\pi\sqrt{L_sC_g}}. \tag{5}$$

In later designs, it is shown that typically $BW_H \gg BW_L$, therefore,

$$\arctan\frac{R_L}{\sqrt{L_s/C_g}} \ll \pi. \tag{6}$$

Thus, the bandwidth expressions can be further simplified,

$$BW_L \approx \frac{R_l}{2\pi L_s}, \tag{7}$$

$$BW_H \approx \frac{1}{2\sqrt{L_sC_g}}. \tag{8}$$

B. Parasitics model

Because the shielded Rogowski coil's performance is directly determined by its parasitic elements, analytical models for these parasitic elements can greatly facilitate the optimization of the coil design. The per-unit-length mutual inductance M' can be written as,

$$M' = \frac{\mu_0 N \left(\sqrt{R+r} - \sqrt{R-r}\right)^2}{2l_w}, \tag{9}$$

where l_w is the wire length of the winding. Unfortunately, there is no explicit closed-form solution to l_w. But it is trivial to obtain by integrating the parametric form of a helix coil,

$$l_w = \int_0^{2\pi} \sqrt{\left(\frac{dx}{dt}\right)^2 + \left(\frac{dy}{dt}\right)^2 + \left(\frac{dz}{dt}\right)^2}\, dt, \tag{10}$$

where $x(t), y(t), z(t)$ are the parametric form of the toroidal helix coil,

$$x(t) = (R + r\cos(nt))\cos(t), \tag{11}$$
$$y(t) = (R + r\cos(nt))\sin(t), \tag{12}$$
$$z(t) = r\sin(nt). \tag{13}$$

The per-unit-length winding-to-shielding capacitance C'_g can be approximated by the wire over ground plane capacitance,

$$C'_g = \frac{2\pi\epsilon_r\epsilon_0}{\operatorname{acosh}\frac{g}{R_w}}, \tag{14}$$

where ϵ_r is the relative permittivity of the insulation material, and R_w is the wire radius of the winding.

The per-unit-length self inductance L'_s is more challenging to calculate accurately. In [11], it is estimated by summing the helix coil inductance and the wire over ground plane inductance,

$$L'_s = \frac{\mu_0 N^2}{l_w}\left(R - \sqrt{R^2 - r^2}\right) + \frac{\mu_0}{2\pi}\operatorname{acosh}\left(\frac{g}{R_w}\right). \tag{15}$$

However, considering the high frequency proximity effect, the magnetic field distribution crowds towards the insulator as the frequency gets higher. So it is difficult to have an accurate estimation of the self inductance L'_s over a wide range of frequencies. On the other hand, the assumption that the helix coil inductance and the wire over ground plane inductance are magnetically orthogonal clearly overestimate the total inductance. According to (3), (7) and (8), the linear transfer impedance, lower and higher bandwidth will all be underestimated.

III. Tilting and Eccentricity Error Analysis

A. Mutual inductance error

Given the parasitic element models in the previous section, it is already possible to formulate an optimization problem on the Rogowski coil design. However, conventional differentiating Rogowski coils suffer from eccentric and tilting errors because of nonuniform or sparse winding [13].

Ideally, the primary side conductor is placed at the center of the Rogowski coil and perpendicularly to the coil plane. However, in reality, the primary side conductor can be tilted and placed at an angle θ with regard to the normal of the coil plane, as shown in Fig. 5. The actual mutual inductance can be found by summing the mutual inductance of each turn, and the expression is given in (16). The number of turns is denoted as N, and $\alpha = \frac{2\pi}{N}$ represents the spanning angle of each turn.

Assuming $R = 10.0$ mm, $r = 0.39$ mm and $g = 0.48$ mm, the sweep of number of turns N, tilt angle θ and the resulting much inductance M over the ideal case M_0 is shown in Fig. 6. When the tilting angle is small $\theta < 60°$, the mutual inductance variation is negligible. However, as the tilt angle becomes larger, higher number of turns N clearly shows better mutual inductance consistency. Specifically, with $N > 30$, the maximum variation is within 10%. Also note that with very large tilt angle $\theta > 80°$, the variation of mutual inductance across different number of turns N shows a somewhat periodic behavior. Therefore, it is possible to choose a number of turns value between the peak and valley points that achieves the lowest variation.

Another non-ideal case occurs when the primary side conductor is placed off-center or eccentrically, as shown in Fig. 7. Similarly, the actual mutual inductance can be found by summing the mutual inductance of each turn. Under the same parameter assumptions as before, the eccentric distance ΔR is swept to understand its impact on the mutual inductance variation. The sweeping result is shown in Fig. 8. Same as the tilting error, the error due to eccentricity becomes negligible when the number of turns is large. Specifically, when the number of turns $N > 30$, the maximum variation is very small and less than 1%.

In conclusion, the mutual inductance variation analysis shows it is preferable to have a higher number of turns. Given the previous parameter assumptions, it is best if the number of turns $N > 30$. The error analysis essentially provides a parameter boundary for the coil design. The final coil design parameters are listed in Table I, and its high frequency performance is shown in Fig. 4.

$$M = \frac{\mu_0}{2\pi}\sum_{i=1}^{N}\int_{R-r}^{R+r} 2\sqrt{r^2-(x-R)^2}\cdot\frac{\cos\theta}{x\sqrt{1-\sin^2\theta\sin^2 i\alpha}\cdot\sqrt{\sin^2\theta\cos^2 i\alpha+\cos^2\theta}}dx. \tag{16}$$

$$M = \frac{\mu_0}{2\pi}\sum_{i=1}^{N}\int_{R-r}^{R+r} 2\sqrt{r^2-(x-R)^2}\cdot\frac{R-\Delta R\cos i\alpha}{R^2+\Delta R^2-2R\Delta R\cos i\alpha}dx. \tag{17}$$

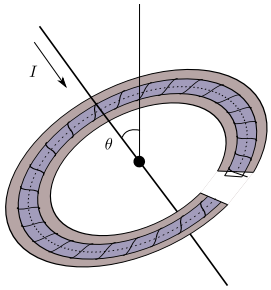

Fig. 5. Tilted primary side conductor in Rogowski coil.

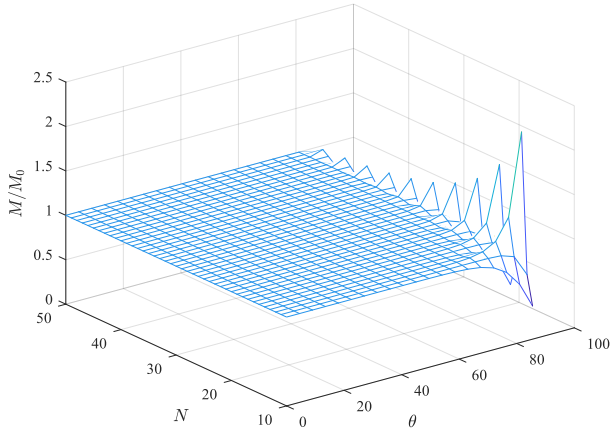

Fig. 6. Variation of mutual inductance when primary side conductor is tilted.

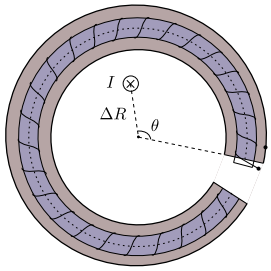

Fig. 7. Eccentric primary side conductor in Rogowski coil

TABLE I. Shielded Rogowski coil design parameters

Parameter	Value
No. of Turns N	34
Major Radius R	10.00 mm
Minor Radius r	0.39 mm
Insulation Gap g	0.48 mm
Load Resistance R_l	2.00 Ω

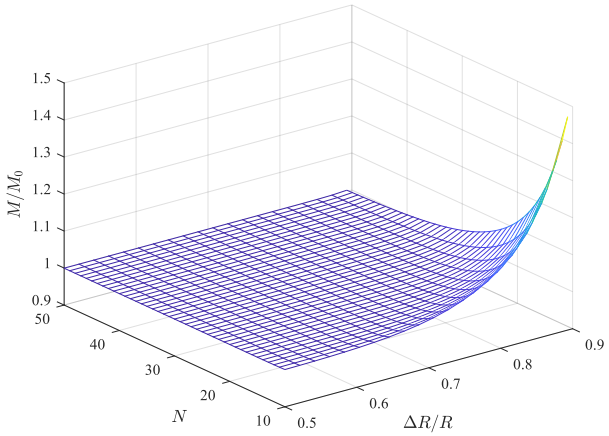

Fig. 8. Variation of mutual inductance when primary side conductor is eccentric.

B. High frequency behavior distortion

Note that in (1), it is assumed that each segment of the distributed circuit shares the same per-unit-length parameters. While this is true for the self inductance L'_s and winding-to-shield capacitance C'_g, it is trivial to see that the mutual inductance M' distribution becomes uneven when the primary side conductor is not placed perpendicularly at the center. To understand the impact from eccentricity to the high frequency behavior, the distributed circuit model is created in SPICE. Each turn is represented as a segment in the distributed circuit.

The transfer impedance Z_t with different eccentric angle θ and eccentric distance ΔR is shown in Fig. 9. In Fig. 9(a), when the primary side conductor is placed perpendicularly at the center of the coil, the high frequency behavior is exactly the ideal case shown in Fig. 4. The higher measurement bandwidth is around 540 MHz. However, as the primary side conductor moves away from the center, as shown in Fig. 9(b) and Fig. 9(d), where $\Delta R = 0.3R$ and $\Delta R = 0.8R$ respectively, the high frequency behavior becomes distorted. The effective higher bandwidth decreased to around 230 MHz by looking at the ± 3 dB point. Furthermore, comparing Fig. 9(b) and Fig. 9(c), where the eccentric angle $\theta = 90°$ and $\theta = 180°$ respectively, the high frequency distortion also depends on the eccentric angle. The case where $\theta = 90°$ is clearly much worse than the case where $\theta = 180°$.

Given the high frequency distortion, it is obvious that the actual usable bandwidth of the shielded Rogowski coil is lower than the ideal value in Fig. 4. This means enough higher bandwidth margin must be kept to ensure the final actual bandwidth is sufficient. On the other hand, it also suggests that if applicable, placing the primary side conductor ideally at the center could significantly increase the overall bandwidth. Also note that this means the winding turns must be evenly distributed, otherwise the uneven mutual inductance distribution would also distort the high frequency behavior.

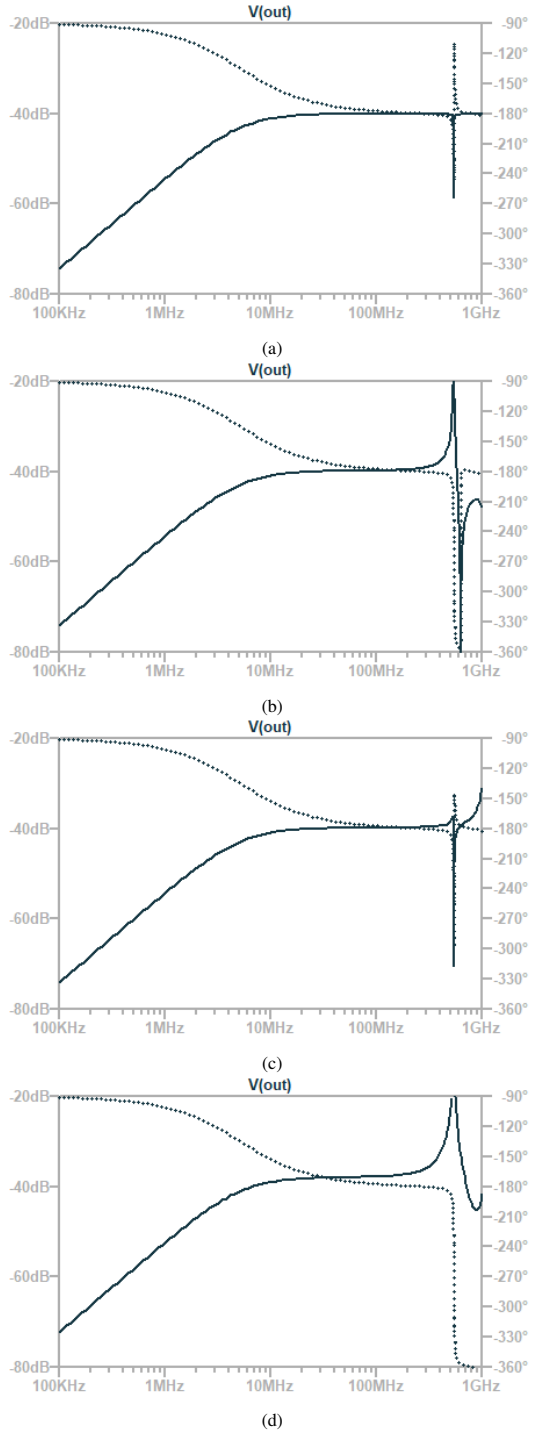

Fig. 9. Rogowski coil eccentricity high frequency distortion: (a) $\theta = 0°, \Delta R = 0$; (b) $\theta = 90°, \Delta R = 0.3R$; (c) $\theta = 180°, \Delta R = 0.3R$; (d) $\theta = 90°, \Delta R = 0.8R$.

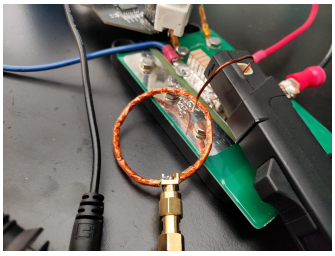

Fig. 10. Combinational Rogowski coil prototype with thin wires and heat-shrink tube.

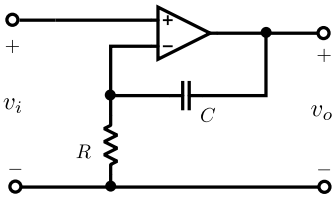

Fig. 11. Non-inverting integrator circuit for analog signal processing.

IV. Coil Fabrication and Verification

A. Coil fabrication

The aforementioned coil is hand built with very thin wires and heat-shrink tubes due to the material availability. The Rogowski coil core is taken from the insulation of a thin wire (AWG24) after stripping the center conductors out. The helix coil winding is made from even thinner wire (AWG32) wound around the insulation core. The insulation gap between the winding and the shielding is made from heat-shrink tube. The heat-shrink tube wall thickness is 0.48 mm. Afterwards, an layer of copper tape is wrapped around the heat-shrink tube. One terminal of the helix winding is soldered to the shielding, while the other terminal and the shielding is connected to a SMA connector. The load resistor is directly soldered between the legs of the SMA connector. Finally, a layer of insulating tape is wrapped around the shielding for electrical isolation. The prototype put into double pulse test to compare its waveform from a commercial current probe (Tektronix TCP0030A) is shown in Fig. 10.

B. Analog signal processing

The concept of combinational Rogowski coil is to utilize both the differentiating and self-integrating region of a shielded coil. The analog signal processing circuit involves integrating the differentiating part, while directly output the self-integrating part. The "hand-off" frequency is the lower bandwidth of the self-integrating region as in (7). A simple non-inverting amplifier circuit is capable of this behavior and is shown in Fig. 11. The transfer function can be trivially found to be

$$G = 1 + \frac{1}{sRC}. \tag{18}$$

However, note that the above behavior is still limited by the op-amp's bandwidth limit. The integrator is implemented with LT6228, which has rail-to-rail output capability. The power

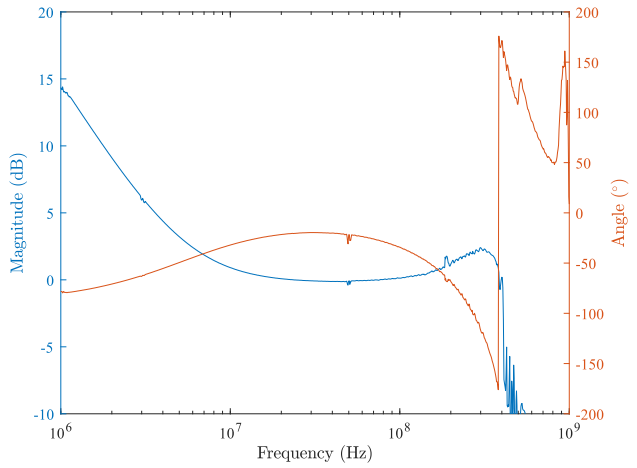

Fig. 12. Non-inverting integrator circuit transfer function measurement.

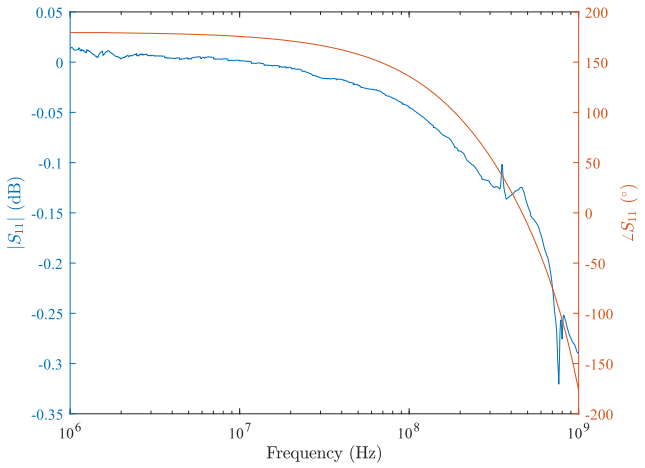

Fig. 14. Measurement chamber S_{11} measurement results showing possible high frequency conversion problem.

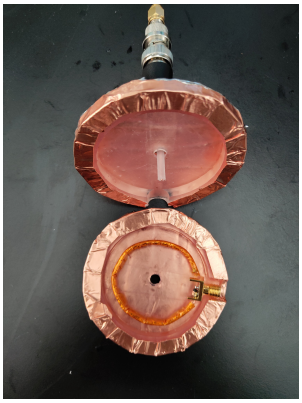

Fig. 13. Measurement setup for the combinational Rogowski coil.

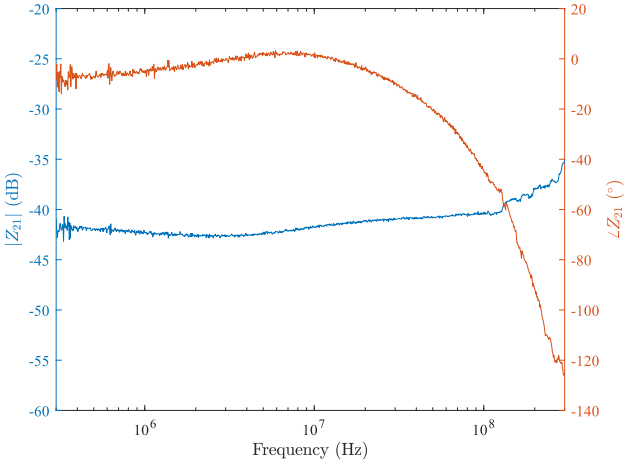

Fig. 15. Combinational Rogowski coil current sensor transfer impedance measurement result.

supply is ± 5.0 V. The transfer function measurement with network analyzer is shown in Fig. 12. The op-amp circuit shows integrating behavior for frequency components below around 5 MHz, and linear 0 dB gain between 5 MHz and 250 MHz. Beyond 250 MHz, the output is limited by the op-amp's bandwidth and starts showing attenuating behavior.

C. Transfer impedance measurement

The transfer impedance measurement of the Rogowski coil, on the other hand, is a lot trickier. A dedicated measurement fixture is built from 3D-printed cylinder chambers, as shown in Fig. 13. The cylinder chamber is wrapped around with copper tape. The BNC cable outer shielding is stripped and connected directly with the outside of the chamber. The center conductor of the BNC cable is threaded through the center of the chamber and connected to the chamber as well. Effectively, a coaxial structure is created where the magnetic filed is restricted within the chamber. The BNC cable is connected to the port 1 and the Rogowski coil sensor output is connected to the port 2 of the network analyzer.

Network analyzers measure *S*-parameters directly and conversion is required to transform them to *Z*-parameters,

$$Z_{21} = \frac{2S_{12}}{(1-S_{11})(1-S_{22}) - S_{12}S_{21}} Z_0, \qquad (19)$$

where $Z_0 = 50\ \Omega$. Because both the measurement chamber and the Rogowski coil are electrically short, at low frequencies, $S_{11} = S_{22} = 1\angle 180°$. However, especially for the measurement chamber, its behavior appears more like an inductor at higher frequencies. Looking at the measurement results of S_{11}, it gets to $1\angle 0°$ at around 540 MHz, as shown in Fig. 14. Therefore, (19) shows the denominator gets close to 0 around 540 MHz, meaning the *S*-to-*Z* conversion is only trustworthy for frequency components below 200 MHz.

The final transfer impedance with the non-inverting integrator connected to the Rogowski coil is shown in Fig. 15. Looking at the ± 3 dB point, the frequency response is relatively flat and around -42 dBΩ or 7.9 mΩ up to around

200 MHz. The flatness is not very good likely due to the "hand-off" frequency not exactly accurate on the non-inverting integrator. Another possible reason is the hand-made Rogowski coil winding density is not well controlled, which may result in non-flat high frequency response. Nevertheless, this shows that the combinational Rogowski coil concept can greatly extend the measurement bandwidth, even with relatively crude hand-made coil.

D. SiC power module double pulse test

The combinational Rogowski coil is first compared with a commercial current probe (Tektronix TCP0030A, 160 MHz, 30 A) to verify the measurement is valid. The measurement setup is shown i Fig. 10. The SiC power module is CAS325M12HM2 (1.2 kV, 3.7mΩ)from Wolfspeed. The comparison between the Rogowski coil and the current probe is shown in Fig. 16. Because the current probe can only measure up to 50 A, the peak current is only around 45 A. The waveforms look very similar between the probe and the Rogowski coil. The noise content in the Rogowski coil is a lot higher than the current probe, but the measurement range of the Rogowski coil is much higher. Given the ± 5 V voltage supply, the range is around ± 630 A.

Finally, to verify that the cross section is small enough that no significant extra power loop inductance is introduced, the double pulse test is performed with either just the Rogowski coil or no current sensor at all. The experimental setup with the Rogowski coil is shown in Fig. 17. A short copper foil is used to connect the decoupling capacitors with the lower device source terminal. When there is no Rogowski coil at all, a flat copper foil is used to make the shorted connection between them. The drain-source voltage V_{ds} waveforms in these two conditions are compared against each other to verify the insertion inductance, as shown in Fig. 18. The difference in the drain-source voltage is very small. The oscillation frequency shift from 27.1 MHz to 25.77 MHz. Therefore, the extra insertion inductance is calculated to be within 2.4 nH.

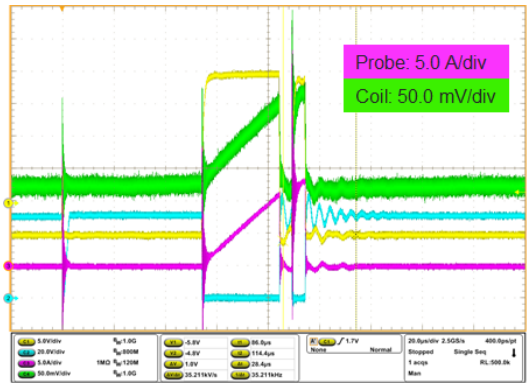

(a)

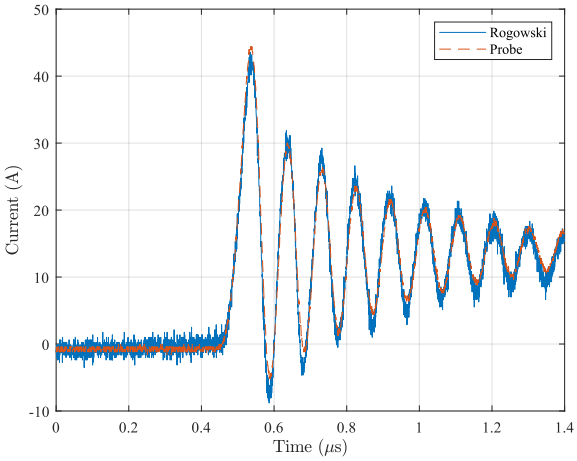

(b)

Fig. 16. Double pulse test waveform comparison between combinational Rogowski coil and commercial current probe: (a) overall comparison; (b) turn-on switching transient comparison.

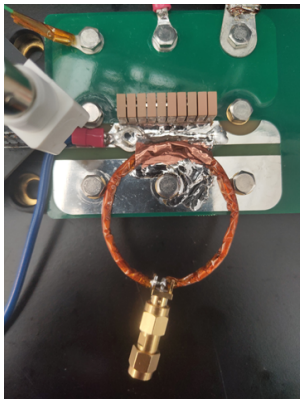

Fig. 17. Double pulse test setup for verifying the extra insertion inductance.

V. Conclusions and Future Work

The concept of combinational Rogowski coil is proposed in this paper. The self-integrating region of shielded Rogowski coils can be utilized to extend the overall measurement bandwidth. The parasitic element models can facilitate the coil design, while the error analysis on eccentricity and tilting provides a design parameter boundary. The concept is implemented by hand with heat-shrink-tube and thin wires. Experimental prototypes demonstrate a measurement bandwidth of more than 200 MHz. Measurement in double pulse test also further confirms the extra insertion inductance is minimal. Therefore, the combinational Rogowski coil proves to be invaluable tool for measuring and monitoring the switching transient current of SiC devices.

Future work will further try to improve the gain flatness, as the gain fluctuates quite a bit in the high frequency. The hand-built fabrication approach is also prone to error and variation,

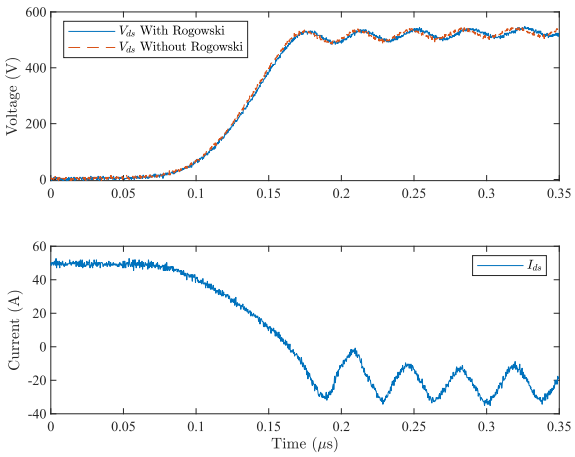

Fig. 18. Drain-source voltage difference with and without the Rogowski coil.

so implementation with automated fabrication process such as printed circuit board is better for more controlled performance.

ACKNOWLEDGMENT

This work was primarily supported by Keysight Technologies through CURENT industry membership. This work made use of Engineering Research Center shared facilities supported by the Engineering Center Program of the National Science Foundation and the Department of Energy under NSF Award Number EEC-1041877 and the CURENT Industry Partnership Program.

REFERENCES

[1] Z. Huang, Y. Li, L. Chen, Y. Tan, C. Chen, Y. Kang, and F. Luo, "A novel low inductive 3D SiC power module based on hybrid packaging and integration method," in *2017 IEEE Energy Conversion Congress and Exposition (ECCE)*, Oct. 2017, pp. 3995–4002.

[2] F. Hou, W. Wang, L. Cao, J. Li, M. Su, T. Lin, G. Zhang, and B. Ferreira, "Review of Packaging Schemes for Power Module," *IEEE Journal of Emerging and Selected Topics in Power Electronics*, vol. 8, no. 1, pp. 223–238, 2020.

[3] Z. Chen, D. Boroyevich, and R. Burgos, "Experimental parametric study of the parasitic inductance influence on MOSFET switching characteristics," in *2010 International Power Electronics Conference - ECCE Asia -, IPEC 2010*, IEEE, 2010, pp. 164–169.

[4] W. Zhang, Z. Zhang, F. Wang, E. V. Brush, and N. Forcier, "High-Bandwidth Low-Inductance Current Shunt for Wide-Bandgap Devices Dynamic Characterization," *IEEE Transactions on Power Electronics*, vol. 8993, no. c, pp. 1–1, 2020.

[5] T&M Research, *Current Viewing Resistors*. [Online]. Available: http://www.tandmresearch.com/.

[6] Pearson Electronics, *Pearson Current Monitor*. [Online]. Available: https://www.pearsonelectronics.com/pdf/7713-03.pdf.

[7] W. Rogowski and W. Steinhaus, "Die Messung der magnetischen Spannung," *Archiv für Elektrotechnik*, vol. 1, no. 4, pp. 141–150, 1912.

[8] M. H. Samimi, A. Mahari, M. A. Farahnakian, and H. Mohseni, "The rogowski coil principles and applications: A review," *IEEE Sensors Journal*, vol. 15, no. 2, pp. 651–658, 2015.

[9] J. Wang, M. H. Hedayati, D. Liu, S. E. Adami, H. C. Dymond, J. J. Dalton, and B. H. Stark, "Infinity Sensor: Temperature Sensing in GaN Power Devices using Peak di/dt," in *2018 IEEE Energy Conversion Congress and Exposition, ECCE 2018*, IEEE, 2018, pp. 884–890.

[10] K. Wang, X. Yang, H. Li, L. Wang, and P. Jain, "A High-Bandwidth Integrated Current Measurement for Detecting Switching Current of Fast GaN Devices," *IEEE Transactions on Power Electronics*, vol. 33, no. 7, pp. 6199–6210, 2018.

[11] V. Dubickas and H. Edin, "High-frequency model of the Rogowski coil with a small number of turns," *IEEE Transactions on Instrumentation and Measurement*, vol. 56, no. 6, pp. 2284–2288, 2007.

[12] I. A. Metwally, "Self-integrating Rogowski coil for high-impulse current measurement," *IEEE Transactions on Instrumentation and Measurement*, vol. 59, no. 2, pp. 353–360, 2010.

[13] G. Zhang and Y. Liu, "Positional error analysis of pcb rogowski coil for high accuracy current measurement," *Advances in Mechanical Engineering*, vol. 2013, 2013.